Int. J. Heat Mass Transfer. Vol. 28, No. 5, pp. 969 976, 1985
Printed in Great Britain

0017 9310/85 $3.00 + 0.00
Pergamon Press Ltd.

Theoretical and experimental study of free convection from a vertical frustum of a cone of a finite length

HITOSHI KOYAMA, AKIRA NAKAYAMA
Department of Mechanical Engineering, Shizuoka University, Hamamatsu, 432 Japan

SEIICHI OHSAWA
Tokyo Sanyo Electric Corporation, Ohizumi, Gunma, Japan

and

HITOSHI YAMADA
Kobe Seiko Corporation, Chiyodaku, Tokyo, 100 Japan

(*Received* 4 *August* 1984 *and in final form* 25 *September* 1984)

Abstract—A theoretical and experimental study has been conducted to investigate free convection from a vertical frustum of a cone of a finite length. Fully elliptic calculation scheme has been proposed to solve the full Navier–Stokes equations. Calculation results are compared with local heat transfer data obtained using a Mach–Zehnder interferometer. A flow visualization has been also attempted using lead stearate powder as a tracer. Both the prediction and measurements suggest that the local heat transfer rate over the lateral surface of the frustum is influenced significantly by the presence of the upper and lower end surfaces of the frustum. It is especially interesting to note that the recirculation region appearing above the upper end surface tends to suppress the diffusion rate of the thermal boundary layer, and consequently leads to a significant augmentation of the local heat transfer rate from the lateral surface.

1. INTRODUCTION

A NUMBER of theoretical studies have been carried out for laminar free convection over plane and axisymmetric bodies. Merk and Prins [1] developed general relations for similarity solutions in the case of axisymmetric flow. Hering and Grosh [2] obtained the similarity solutions for a vertical cone when the wall temperature distribution is in a form of a power function of distance along a cone ray. These similarity solutions assume transverse radial curvature effects to be negligible. Thus, results are inevitably in error near the apex of a cone, where the boundary-layer thickness is comparable to the radius of the transverse curvature. Kuiken [3] proposed a perturbation procedure to consider the curvature effects on the heat transfer rate, and showed that the effects are, in fact, quite significant especially for slender cones.

All the above analyses are based on the boundary-layer approximations. However, during actual free convection processes, the elliptic nature of the flow may become evident. In consideration of this fact, Kuehn and Goldstein [4], Farouk and Güceri [5] and Fujii *et al.* [6] attempted to solve the full Navier–Stokes equations for the analysis of free convection from a horizontal circular cylinder. Subsequently, the authors [7] used the Navier–Stokes equations to simulate the actual free convection flow around a vertical cone in a sealed laboratory, and showed that recirculation bubbles form above the upper end surface of the cone, which consequently leads towards a significant augmentation of the local heat transfer rate.

As for an axisymmetric configuration, a vertical frustum of a cone of a finite length as depicted in Fig. 1, has been selected for the present investigation. The free convection flow over a heated frustum exhibits many interesting features. Stagnant flow appears on the lower end surface of the frustum facing downward, while a recirculation zone may be expected above the upper end surface when the Grashof number is sufficiently high. Therefore, it is natural to expect that the flow fields on both upper and lower end surfaces affect the heat transfer characteristics over the lateral surface of the frustum. Na and Chiou [8] studied analytically free convection over a frustum of a cone using a quasi-linearization method. The frustum of a cone was assumed to have an infinite length, and usual boundary-layer approximations were adopted. Hence, their analysis does not consider either the stagnant flow on the lower end surface nor the recirculating flow above the upper end surface. However, in the actual case of the frustum of a finite length, parabolic approximations are hardly valid, as pointed out in the study of a cone with a closed end [7]. In the present work, the full Navier–Stokes equations are solved to investigate the elliptic nature of the free convection flow around a frustum of a cone of finite length, with special emphasis on the local heat transfer from the lateral surface of the frustum.

In the experimental part of the present study, an effort was made to determine the heat transfer rate

NOMENCLATURE

g	acceleration of gravity
Gr_L	$g\beta(T_w-T_\infty)L^3\cos\alpha/\nu^2$, Grashof number based on L
Grx_b	$g\beta(T_w-T_\infty)x_b^3\cos\alpha/\nu^2$, Grashof number based on x_b
h	local heat transfer coefficient
k	thermal conductivity
L	slant height of the frustum
Nux_b	hx_b/k, local Nusselt number
p	pressure
Pr	Prandtl number
r_0	radius of lower end surface
r_s	radius of rod
T	temperature
u, v	velocity components in cylindrical coordinates
u_b	velocity component in x_b direction
u_{ref}	$[g\beta(T_w-T_\infty)L]^{1/2}$, reference velocity
x, r	cylindrical coordinates
x_b, y_b	boundary-layer coordinates.

Greek symbols

α	frustum slant angle
β	coefficient of thermal expansion
Γ	general diffusion coefficient
ν	kinematic viscosity
ρ	density
ϕ	general dependent variable.

Subscripts

w	wall
∞	ambient.

locally by means of a Mach–Zehnder interferometer. The heat transfer data deduced from interferograms indicates significant effects of both upper and lower end surfaces on the local heat transfer rate over the lateral surface of the frustum. A flow visualization was also conducted to resolve recirculation bubbles appearing above the upper end surface.

Thus, the purpose of the present paper is to discuss the complex phenomenon of the free convection from a frustum of a cone of a finite length through a careful comparison of prediction and experiment.

2. PHYSICAL MODEL AND GOVERNING EQUATIONS

The physical model under consideration is depicted in Fig. 1. A frustum of a cone with slant angle α, slant height L and a radius of the lower end surface r_0 is attached to a rod with a radius r_s, and suspended vertically downward from a ceiling of a large sealed room. While the boundary-layer coordinates (x_b, y_b) are used for the interpretation of the temperature and velocity fields along the cone ray, the numerical calculations are carried out using the cylindrical coordinate system (x, r) with its origin located at the center of the lower end surface as indicated in the figure.

By employing the Boussinesq approximation for the buoyancy force, all the governing equations may be expressed in a general form as

$$\frac{\partial}{\partial x}r\left(u\phi-\Gamma\frac{\partial\phi}{\partial x}\right)+\frac{\partial}{\partial r}r\left(v\phi-\Gamma\frac{\partial\phi}{\partial r}\right)=so. \quad (1)$$

Each governing equation is then given by setting ϕ, Γ and so as follows:

For the continuity equation,

$$\phi=1,\quad \Gamma=0,\quad so=0. \quad (2a)$$

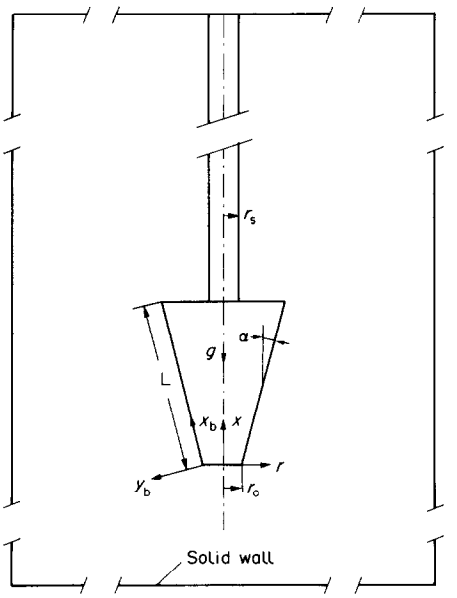

FIG. 1. Physical model and coordinates.

For the u momentum equation,

$$\phi=u,\quad \Gamma=\nu,$$

$$so=-\frac{r}{\rho}\frac{\partial}{\partial x}(p+\rho gx)+rg\beta(T-T_\infty). \quad (2b)$$

For the v momentum equation,

$$\phi=v,\quad \Gamma=\nu,$$

$$so=-\frac{r}{\rho}\frac{\partial}{\partial r}(p+\rho gx)-\nu\frac{v}{r}. \quad (2c)$$

For the energy equation,

$$\phi=T,\quad \Gamma=\nu/Pr,\quad so=0. \quad (2d)$$

In the above equations, u and v are the velocity components in the x and r directions while T and p denote the temperature and the pressure. The density, kinematic viscosity and the Prandtl number are indicated by ρ, ν and Pr respectively. The buoyancy term contains the thermal expansion coefficient β and the acceleration due to gravity g.

3. DESCRIPTION OF NUMERICAL SCHEME

Following the procedure suggested by Pope and Whitelaw [9], equation (1) has been discretized by integration within a finite control volume. As proposed by Patankar and Spalding [10], the continuity equation (2a) has been reformulated into the pressure correction equation. This correction procedure requires a staggered grid arrangement, in which velocities are defined midway between the pressure nodes. Calculations start with solving u and v momentum equations (2b) and (2c), and subsequently, this estimated velocity field is corrected by solving the pressure correction equation so that the velocity field fulfills the continuity principle. Details of this pressure correction procedure may be found in the original paper by Patankar and Spalding [10].

Many workers (e.g. [11, 12]) suggested the use of coordinate transformations for the treatment of irregular boundaries such as those shown in Fig. 1 for the present configuration, which consists of end surfaces, a slanted lateral surface, a string surface and room wall surfaces. Although the coordinate transformation enables one to locate all available grid nodes within the flow field, the source program often requires considerable modification each time for even a slight change in the geometrical configuration. In order to achieve universality of the computer code, Nakayama *et al.* [7, 13] suggested a procedure which retains the conventional cylindrical coordinate system, and distributes grid points such that the straight boundaries are located midway between the pressure nodes. This also applies to the slanted boundary along the cone ray (thus, the spacing of the nodes is maintained in the two directions in the ratio of 1 : tan α). This procedure, when used with the staggered grid system, leads to considerable simplification of the treatment of irregular boundaries. Details of the procedure may be found elsewhere [13].

One half of the meridian plane on the left of the axis of symmetry is taken for the calculation domain. For the velocity boundary conditions, all solid surfaces are subjected to no-slip conditions, while usual symmetry conditions are employed along the axis of symmetry below the lower end surface of the frustum. In consideration of the actual experimental conditions, the surface temperatures of the room wall, the pole and the upper end surface of the frustum are all set to a constant temperature T_∞, while those of the lateral surface and the lower end surface are set to a higher temperature T_w. The symmetry condition $\partial T/\partial r = 0$ is imposed along the axis of symmetry.

Preliminary calculation results indicated that the size of the calculation domain becomes immaterial to both the velocity and temperature fields around the frustum when the domain is as large as $-1.2 \leqslant x/L \leqslant 10$, and $0 \leqslant r/L \leqslant 10\,(r_0/L + \sin\alpha)$. All dependent and independent variables are normalized by the reference length L and the reference velocity $u_{ref} = [g\beta L(T_w - T_\infty)]^{1/2}$. For given geometrical parameters ($\alpha, r_0/L, r_s/L$, etc.), Prandtl number Pr and Grashof number $Gr_L = \cos\alpha$, calculations have been carried out using the grid nodes (55×55) with highly non-uniform grid spacings so that the region around the frustum will have finer meshes. Convergence was measured in terms of the maximum change in each variable during an iteration. The maximum change allowed for the convergence check was set to 10^{-6}.

4. EXPERIMENTAL PROCEDURE

A frustum of a cone made of brass with $\alpha = 15°$, $L = 103.3$ mm and $r_0 = 12$ mm, is connected to a rod of radius $r_s = 10$ mm, and suspended vertically in a sealed laboratory of a large volume (100 m^3). The frustum is heated to a constant temperature above the ambient air temperature (in the range of $45 \leqslant T_w - T_\infty \leqslant 70°C$) using two nichrome heaters which are imbeded under the lateral and lower end surfaces of the frustum, and controlled independently of each other to maintain the temperatures of the lateral and lower end surfaces as uniform as possible. The temperature measurement made at various points using copper–constantan thermocouples imbedded in the frustum, confirmed that the temperatures over the lateral and lower end surfaces were kept nearly uniform all over except the region near the upper end surface made of bakelite, where the temperature was found to drop slightly (1–2°C).

Local heat transfer measurements are carried out using the interferometric technique. Fringe displacement numbers are read from Mach–Zehnder interferograms, and the linearized version of the Lorenz–Lorentz formula is employed for the reduction of the temperature field around the frustum (see e.g. [14]). Consequently, the heat transfer rate over the lateral surface is determined locally by reading the temperature gradient at the surface. During the experiment, all precautions have been taken to avoid flow disturbances by such as vibrations and stray convections.

A flow visualization was also attempted using fine lead stearate powder as a tracer. The frustum of a cone is placed in the centre of a large box (10 m^3). Tracer particles of diameter in the range of 2 to 5 μm were supplied for 10 min from the bottom of the box at velocities as low as 5 mm s^{-1}. Then, the box is sealed completely, and kept still for about 1 h so that the particles attain uniform distribution before actual measurements start. This flow visualization technique

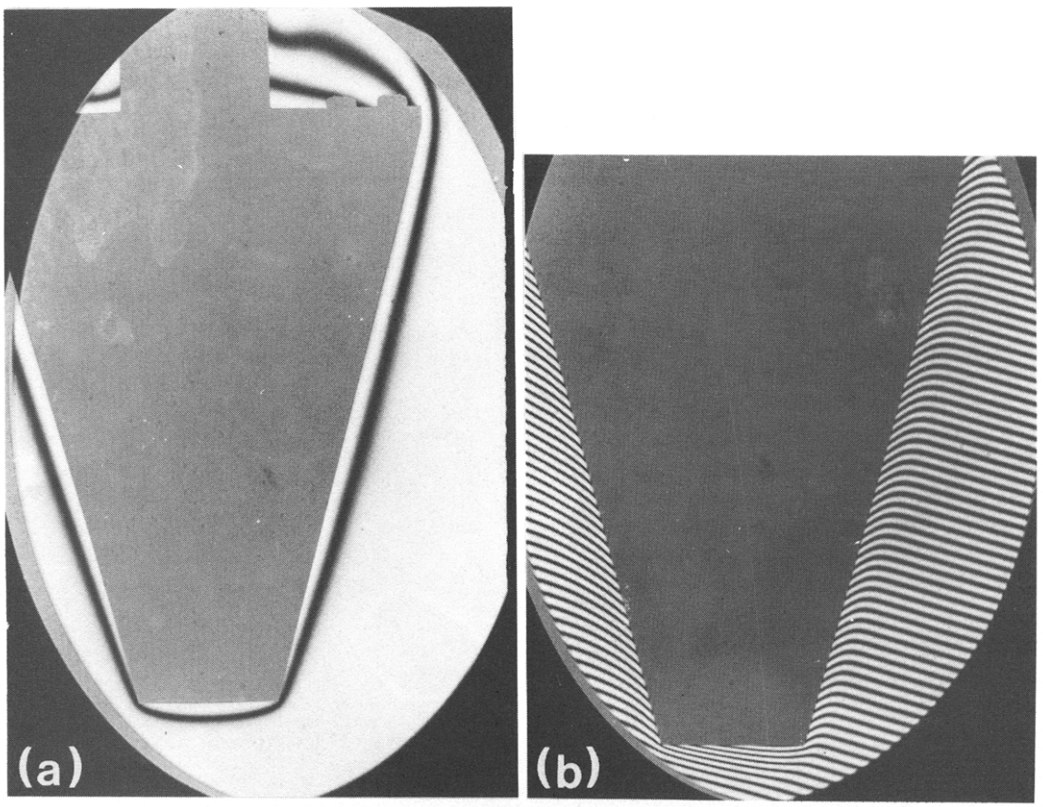

FIG. 2. Interferograms: (a) infinite fringe mode; (b) wedge fringe mode.

is essentially the same as the one employed by Aihara and Sato [15] for the study of free convection. The procedure has been reported in detail in their paper.

5. RESULTS AND DISCUSSIONS

5.1. *Interferograms for temperature field*

A typical interferogram obtained by an infinite fringe mode is shown in Fig. 2(a) for $Gr_L = 5.5 \times 10^6$ ($T_w - T_\infty \cong 50°C$). The development of the thermal boundary layer around the frustum is clearly seen. The fringe over the lower end surface exhibits a pattern characteristic of a stagnant layer. For quantitative measurements of local heat transfer over the lateral surface, a wedge fringe mode was employed adjusting the mirrors of the interferometer so that the fringes outside the thermal boundary layer extend perpendicular to the cone ray, as shown in Fig. 2(b).

As observed from both Figs. 2(a) and 2(b), the thickness of the thermal boundary layer is already appreciable on the leading edge of the lateral surface at $x_b = 0$. Naturally, a considerable influence of the lower end surface may be expected on the subsequent flow development along the lateral surface. It is seen in Fig. 2(a) that the thermal boundary layer initially thickens downstream away from $x_b = 0$, as in a usual boundary-layer development, but it gradually becomes thinner as it approaches the trailing edge at $x_b = L$. As the diffusion rate of the thermal boundary layer is suppressed, a higher transfer rate can be achieved toward the trailing edge.

5.2. *Calculation results of heat transfer rate*

In order to investigate further the effects of the lower and upper end surfaces on the local heat transfer from the lateral surface, the full Navier–Stokes equations have been solved numerically using the aforementioned numerical procedure. Then, the calculation results are transformed into the boundary-layer coordinates (x_b, y_b). The local heat transfer rate thus determined along the cone ray $0 \leqslant x_b/L \leqslant 1$, is indicated in Fig. 3, where the ordinate variable is chosen to provide a direct comparison with the Hering and Grosh's similarity solution [2], namely, $Nux_b/Grx_b^{1/4} = 0.451$ for $Pr = 0.7$ (where $Nux_b = hx_b/k$ and $Grx_b = g\beta(T_w - T_\infty)x_b^3 \cos\alpha/\nu^2$).

For comparison, calculations have been carried out for a cone of a finite length with an apex angle 15° and for the same Gr_L. The results are presented in the same figure along with the Kuiken's perturbation solution obtained for a cone of an infinite length. Both the present solution and Kuiken's solution for a cone indicate significant radial curvature effects on the local heat transfer rate especially near the apex of a cone, as manifested by a steep heat transfer increase there. As x_b/L becomes large, the Kuiken's perturbation solution asymptotically approaches the level of the similarity solution, while the present fully elliptic solution (which

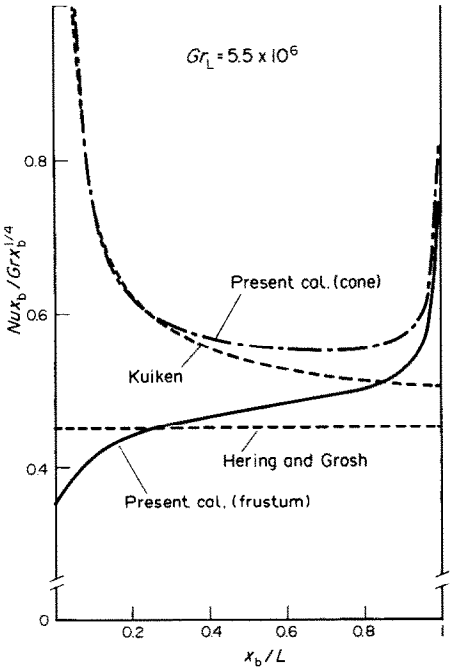

FIG. 3. Calculation results of local heat transfer.

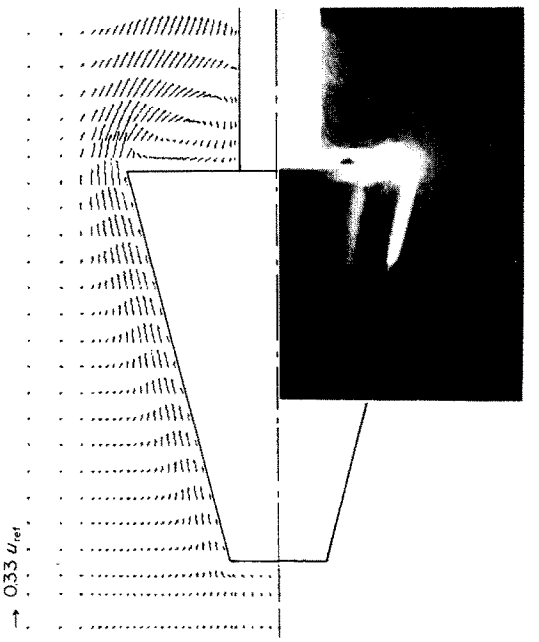

FIG. 4. Velocity field around a frustum.

is in good accord with the Kuiken's solution near the apex) gives a steep increase toward the trailing edge at $x_b/L = 1$.

In contrast with considerable heat transfer increase toward $x_b = 0$ as a result of the radial curvature of the cone, the local heat transfer rate near the leading edge ($x_b = 0$) of the lateral surface of the frustum appears to be even less than that of the similarity solution. This moderate heat transfer rate near the leading edge may be regarded as a direct consequence of the stagnant flow induced over the lower end surface [see Fig. 2(a)]. In other words, the presence of the lower end surface smears the radial curvature effects and prompts the radial diffusion of the thermal boundary layer, consequently leading to a decrease in the heat transfer rate near the leading edge of the lateral surface of the frustum. But, away from the leading edge, $Nux_b/Grx_b^{1/4}$ increases gradually and exceeds the level of the similarity solution. Closer to the trailing edge, the heat transfer rate increases sharply as in the case of the cone of a finite length. This phenomenon is consistent with the experimental evidence seen in Fig. 2(a), namely, the decrease in the thermal boundary-layer thickness near the trailing edge. The suppression of the thermal diffusion toward the trailing edge cannot be explained without considering the flow field over the upper end surface.

5.3. *Comparison of experiment and prediction*

In Fig. 4, the predicted velocity vector plot is presented with a photograph taken during the flow visualization using lead stearate powder. Both the prediction and experiment clearly indicate the existence of the recirculation zone.* It is interesting to see that fluids passing over the trailing edge are continuously drawn into the recirculation region. As a result, the diffusion of the boundary layer is delayed, hence, relatively high heat transfer rate can be attained toward the trailing edge, for the thermal resistance there is kept low.

Local heat transfer results reduced from the wedge fringe mode interferograms are compared with the present elliptic calculation results in Fig. 5. The parabolic calculation results obtained by matching the solutions for the lower end surface and for the lateral surface [17] are also presented in the figure by a dashed line. The level predicted by the present elliptic calculation procedure is everywhere higher than that by the parabolic calculation procedure, and appears to be in good agreement with the experiment. Data points near the edges are not shown in the figure since the reading of the fringe displacement number turned out to be extremely difficult near the leading and trailing edges due to insufficient resolution in the interferograms. However, although qualitatively, the infinite fringe mode interferogram in Fig. 2(a) does substantiate the drastic heat transfer increase near the trailing edge as in the prediction.

Furthermore, the comparison of the elliptic and parabolic calculation results reveals that the presence of the recirculation zone above the upper end surface

*The authors are grateful to Prof. E. Saito of Iwate University who brought our attention to the experimental study [16] by his group on the recirculation bubble above a heated cone of a finite length.

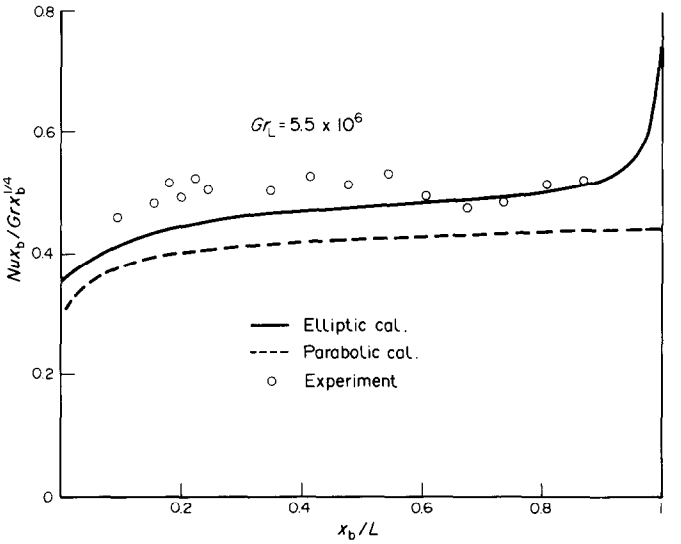

FIG. 5. Comparison of prediction and experiment.

increases the heat transfer rate not only within the region close to the trailing edge, but also far upstream. In fact, its elliptic effect on the heat transfer enhancement seems to prevail almost over the entire lateral surface of the frustum. This phenomenon is quite interesting when one contrasts it with the fact usually true in the forced convective heat transfer, namely, that the influence of the flow separation on the temperature field is restricted to the region near the separated region, and the boundary layer concept still holds upstream of the separation point. In contrast with the above consideration in the forced convection, this rather surprising elliptic interaction between the velocity and temperature fields is possibly associated with the strong coupling effect between the momentum and energy equations through the buoyancy terms, hence, appears

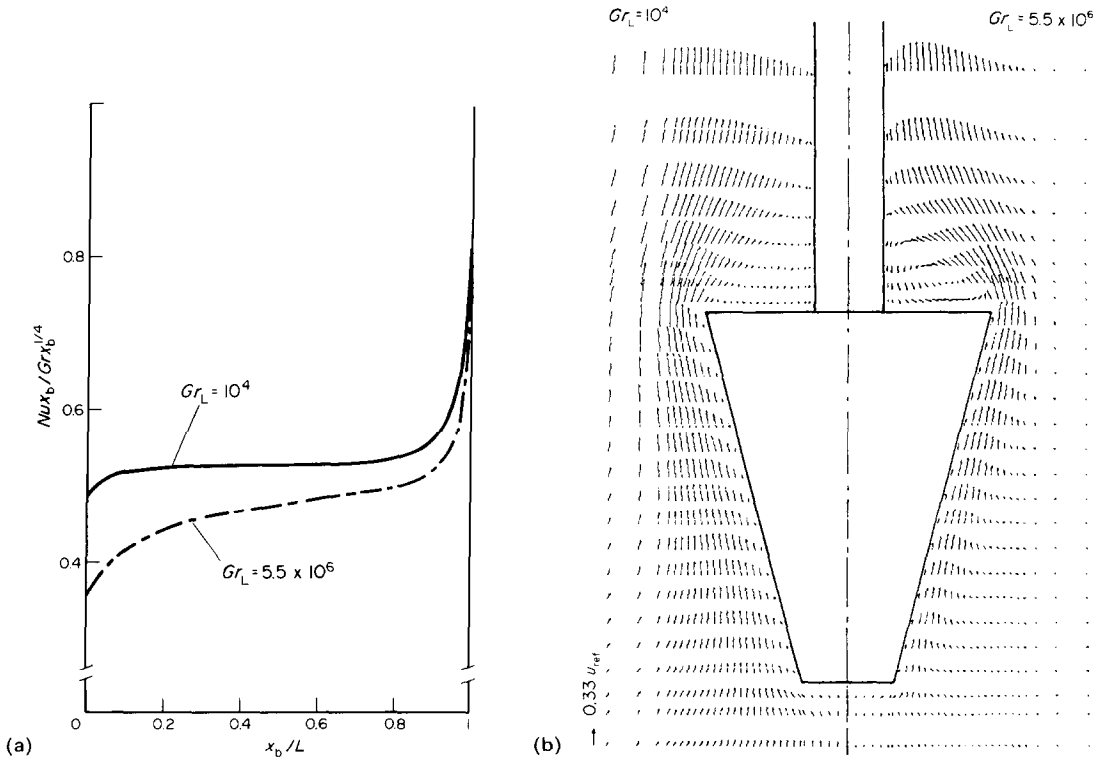

FIG. 6. Grashof number effects: (a) local heat transfer; (b) velocity field.

to be characteristic of the free convection flows of this kind.

5.4. *Grashof number effects*

In order to investigate the Grashof number effects on the local heat transfer from a lateral surface of a frustum, elliptic calculations have been also carried out for the case of moderate Grashof number, namely, $Gr_L = 10^4$. Results on the local heat transfer rate over the lateral surface are plotted in Fig. 6(a) with those obtained for $Gr_L = 5.5 \times 10^6$.

It is clearly seen that the level of $Nux_b/Grx_b^{1/4}$ becomes high as Gr_L decreases. This level increase is appreciable especially near the leading edge of the lateral surface. The observed trend is obviously associated with the aforementioned effects of transverse radial curvature on the local heat transfer. As Gr_L becomes less, the ratio of the boundary-layer thickness to the local radius of transverse curvature (corresponding to the Kuiken's perturbation parameter) increases at the rate of $Gr_L^{-1/4}$. Thus, a rather high level of $Nux_b/Grx_b^{1/4}$ is maintained near the leading edge despite the fact that the stagnant layer on the lower end surface tends to smear the radial curvature effects to some extent.

The Grashof number effects on the velocity field around the frustum may be seen in Fig. 6(b) which presents the velocity vector plot for $Gr_L = 10^4$ on the left and that for $Gr_L = 5.5 \times 10^6$ on the right, respectively. While the boundary layer grows thick for the smaller Gr_L, the flow patterns for both cases appear to be very much similar. Since the recirculation zone also forms for the case of $Gr_L = 10^4$, the heat transfer rate is expected to increase towards the trailing edge as in the case of high Gr_L [see Figs. 6(a) and 6(b)]. A comparison of the velocity vector plots within a recirculation region, however, reveals that the decrease in Gr_L lowers the back flow velocity magnitude significantly.

6. CONCLUDING REMARKS

Free convection flows induced over smooth closed bodies such as horizontal cylinders and spheres, usually do not separate (in contrast with forced flows) since the buoyancy force works favorably everywhere, driving fluids upward. It has, however, been pointed out through the present study, that, even in free convection flows, the recirculation zones can be formed when the heated body possesses a sharp trailing edge, as in the present case of a frustum of a cone of a finite length. Once a recirculation bubble appears, its influence does not remain locally, but extends far upstream over the lateral surface of the body. It is especially interesting to note that this elliptic nature in the free convection flow can contribute significantly towards augmentation of the local and overall heat transfer rates.

Acknowledgements—The authors would like to express their sincere thanks to Mr. E. Makita, Mr. T. Ishii and Mr. K. Hattori for their invaluable contributions in the experiment. Special thanks are also due to Mr. M. Suzuki for skillful development and printing of films. All numerical calculations have been carried out at the Computer Center of Shizuoka University in Hamamatsu.

REFERENCES

1. H. J. Merk and J. A. Prins, Thermal convection in laminar boundary layers, *Appl. scient. Res.* **A4,** 11–24 (1953).
2. R. G. Hering and R. J. Grosh, Laminar free convection from a non-isothermal cone, *Int. J. Heat Mass Transfer* **5,** 1059–1068 (1962).
3. H. K. Kuiken, Axisymmetric free convection boundary-layer flow past slender bodies, *Int. J. Heat Mass Transfer* **11,** 1141–1153 (1968).
4. T. H. Kuehn and R. J. Goldstein, Numerical solution to the Navier–Stokes equations for laminar natural convection about a horizontal isothermal circular cylinder, *Int. J. Heat Mass Transfer* **23,** 971–979 (1980).
5. B. Farouk and S. I. Güceri, Natural convection from horizontal cylinders in interacting flow fields, *Int. J. Heat Mass Transfer* **26,** 231–243 (1983).
6. T. Fujii, M. Fujii and T. Honda, Theoretical and experimental studies on the free convection around a horizontal long thin wire in air, in Japanese, *Trans. Japan Soc. Mech. Engng.* **48-431,** 1312–1320 (1982).
7. A. Nakayama, H. Koyama and S. Ohsawa, Free convection from a cone with a Closed End, *Letters Heat Mass Transfer* **9,** 455–462 (1982).
8. T. Y. Na and J. P. Chiou, Laminar natural convection over a slender vertical frustum of a cone, *Wärme Stoffübertr.* **12-2,** 83–88 (1979).
9. S. B. Pope and J. H. Whitelaw, The calculation of near-wake flows, *J. Fluid Mech.* **73,** 9–32 (1976).
10. S. V. Patankar and D. B. Spalding, A calculation procedure for heat, mass and momentum transfer in three-dimensional parabolic flows, *Int. J. Heat Mass Transfer* **15,** 1787–1806 (1972).
11. S. B. Pope, The calculation of turbulent recirculating flows in general orthogonal coordinates, *J. Comput. Phys.* **26,** 197–217 (1978).
12. A. Nakayama, W. L. Chow and D. Sharma, Calculation of fully developed turbulent flows in ducts of arbitrary cross section, *J. Fluid Mech.* **128,** 199–217 (1983).
13. A. Nakayama, H. Koyama and S. Ohsawa, Theoretical and experimental study of turbulent separated flows behind a rotating axisymmetric body, *Numer. Heat Transfer* **7,** 359–371 (1984).
14. M. Jakob, *Heat Transfer*, Vol. II, pp. 577–587. John Wiley, New York (1959).
15. T. Aihara and E. Sato, Measurement of free convection velocity field around the periphery of a horizontal torus, *J. Heat Transfer*, **94,** 95–101 (1972).
16. E. Saito, Y. Naganuma, T. Yoshino and F. Saito, Natural convection from two cones in line arrangement vertically, *Proc. 18th HTSJ Symposium*, pp. 328–330, in Japanese (1981).
17. H. Yamada, Free convection around a vertical frustum of a cone, M. S. thesis, Shizuoka University, in Japanese (1983).

ETUDE THEORIQUE ET EXPERIMENTALE DE LA CONVECTION NATURELLE A PARTIR D'UN TRONC DE CONE VERTICAL DE LONGUEUR FINIE

Résumé—Une étude théorique et expérimentale aborde la convection naturelle à partir d'un tronc de cone vertical de longueur finie. Un schéma de calcul elliptique est proposé pour résoudre les équations de Navier–Stokes. Les résultats du calcul sont comparés aux données de transfert thermique local obtenues par interférométrie Mach–Zehnder. Une visualisation d'écoulement a été faite en utilisant de la poudre de stearate de plomb comme traceur. Les calculs et les mesures suggèrent que le flux de chaleur local sur la surface latérale est fortement influencé par la présence des surfaces supérieure et inférieure du tronc de cône. On note spécialement que la région de recirculation apparait au dessus de la surface supérieure et qu'elle tend à supprimer le flux de diffusion de la couche limite thermique et par conséquent conduit à une augmentation sensible du flux thermique local sur la surface latérale.

THEORETISCHE UND EXPERIMENTELLE UNTERSUCHUNG DER FREIEN KONVEKTION AN EINEM SENKRECHTEN KEGELSTUMPF VON ENDLICHER LÄNGE

Zusammenfassung—Die freie Konvektion an einem senkrechten Kegelstumpf von endlicher Länge wurde theoretisch und experimentell untersucht. Um die vollständigen Navier–Stokes-Gleichungen zu lösen, wurde ein voll-elliptisches Berechnungsmodell angesetzt. Die Ergebnisse der Berechnung wurden mit den örtlichen Wärmeübergangsdaten verglichen, die mit Hilfe eines Mach–Zehnder-Interferometers ermittelt worden waren. Die Strömung wurde mit Hilfe von Blei-Stearat-Puder sichtbar gemacht. Sowohl die Berechnungen als auch die Messungen zeigten, daß der örtliche Wärmeübergang des Kegelmantels stark von dem Vorhandensein der oberen und unteren Abschlußfläche abhängt. Besonders bemerkenswert ist, daß das Rückströmgebiet über der oberen Abschlußfläche dazu neigt, die Diffusion in der thermischen Grenzschicht zu unterdrücken, was zu einer bemerkenswerten Verbesserung des örtlichen Wärmeübergangs an der Mantelfläche führt.

ТЕОРЕТИЧЕСКОЕ И ЭКСПЕРИМЕНТАЛЬНОЕ ИССЛЕДОВАНИЕ СВОБОДНОЙ КОНВЕКЦИИ ОТ ВЕРТИКАЛЬНОГО УСЕЧЕННОГО КОНУСА КОНЕЧНОЙ ДЛИНЫ

Аннотация—Теоретически и экспериментально изучена свободная конвекция от вертикального усеченного конуса конечной длины. Для решения полных уравнений Навье Стокса предложена эллиптическая схема расчета. Результаты сравниваются с данными по местному теплообмену, полученными с помощью интерферометра Маха–Цандера. Для визуализации течения применялся порошок стеариновокислого свинца. В результате расчетов и измерений показано, что на коэффициент местной теплоотдачи от боковой поверхности существенно влияют верхняя и нижняя торцевые поверхности усеченного конуса. Интересно отметить, что циркуляционная зона, возникающая над верхним торцом, скорость размывания теплового пограничного слоя и приводит к существенному увеличению коэффициента местного теплообмена с боковой поверхности.